Ninth International Conference on
THIN-WALLED STRUCTURES – ICTWS2023
Sydney, Australia, Nov 29 – Dec 1, 2023

DAMAGE DETECTION IN CONICAL SHELLS USING AN INVERSE FINITE ELEMENT BASED ON GENERALISED BEAM THEORY

Ionel D. Craiu[1], Mihai Nedelcu[2]

[1,2] Department Structural Mechanics, Faculty of Civil Engineering, Technical University of Cluj-Napoca, Romania
e-mails: Ionel.Craiu@mecon.utcluj.ro, Mihai.Nedelcu@mecon.utcluj.ro

Keywords: Conical shells; Inverse Finite Element Method; Generalised Beam Theory; Strain sensors; Shape sensing; Damage detection.

Abstract. *The offshore industry frequently employs thin-walled conical shells with circular cross-sections as columns of floating structures. When it is not possible to directly identify specific structural deformations, the inverse Finite Element Method (iFEM) can do so based on measured strains. Structural Health Monitoring makes considerable use of this technology. However, the solution depends on the number of in-situ strain gauges, and for shell structures with complex deformation, a high number will make the method unpractical. Generalized Beam Theory (GBT) uses a linear superposition of cross-section deformation modes to describe the behaviour of thin-walled members with arbitrary cross-sections. Being a bar theory, GBT uses a lot fewer degrees of freedom than the typical shell finite element analysis. An iFEM/GBT formulation for isotropic conical shells with circular cross-sections is presented in this study. Using discrete strains measured on the member surface, the deformation is replicated, and damage detection is performed by comparing the strain distributions of the undamaged and damaged members.*

1 INTRODUCTION

This paper presents an innovative approach for monitoring floating offshore or land wind turbines, focusing on the shape sensing and detection of potential damage for the thin-walled conical elements acting as columns to such structures. Shape sensing involves the real-time estimation of the deformed shape, using strains measured by a grid of on-board sensors (e.g., strain gauges or fiber Bragg grating strain sensors). The procedure is an extension of the shape sensing formulation recently developed by Nedelcu [1] for thin-walled cylinders, and it is based on the inverse Finite Element Method (iFEM) originally developed by Tessler and Spangler ([2], [3]), combined with the Generalized Beam Theory (GBT) [4]. GBT is a bar theory that has the capability to represent the deformation of thin-walled members by expressing it as a linear combination of predefined cross-section deformation modes, while iFEM can find the degrees of freedom (DOF) and consequently reconstruct the displacement/strain field, by minimizing the differences between measured and theoretical strains. The proposed iFEM/GBT formulation uses a new 1D inverse FE, significantly reducing the DOF number and consequently the strain points, in comparison with the conventional shell iFEM, as demonstrated in [1] .

Moreover, Li et al. [5] developed a damage detection method considering the differences between the reconstructed strains on the undamaged and damaged structure. The proposed damage parameter will be used in this paper as well, in combination with iFEM/GBT. The proposed formulation is validated through numerical examples where the experimentally measured strains are simulated by strains obtained from shell FE analyses.

2 GBT FOR CONICAL SHELLS

Figure 1 illustrates the configuration of a conical element, characterized by its length (L), thickness (t), and semi-vertex angle (α). The coordinate systems include the global coordinate system (X, Y, Z) and the local coordinate system (x, θ, z). By employing Kirchhoff's thin plate assumption, the displacements of the shell are derived from the mid-surface displacements. Specifically, the meridional, circumferential and transversal displacements along the local axes are represented by *u*, *v* and *w* respectively.

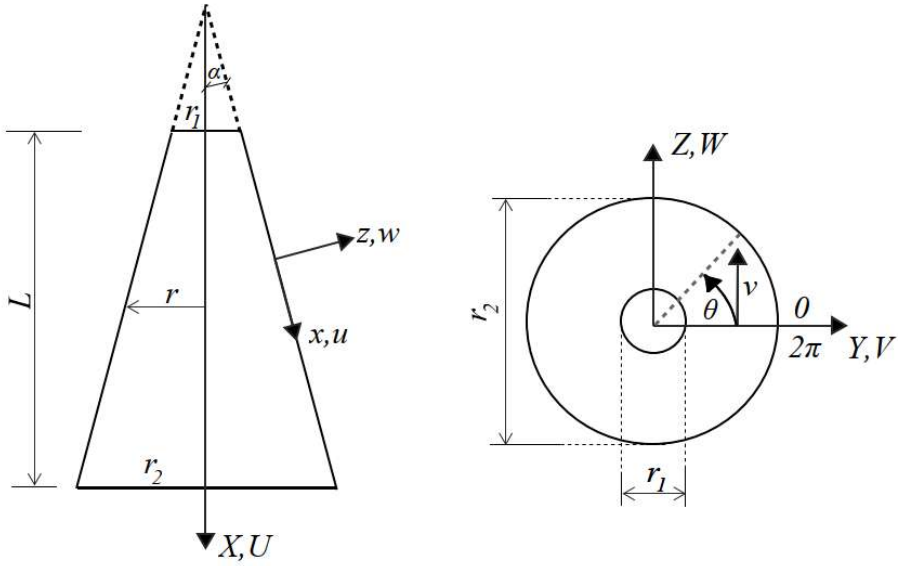

Figure 1: The components of displacements in the local and global coordinate system.

2.1 Linear kinematic relations

According to the Love-Timoshenko theory, the linear kinematic relations in the case of conical shells are expressed by Eqs. (1-3) [6], considering the notations *s=sin(α)* and *c=cos(α)*.

$$\varepsilon_{xx} = u_{,x} - zw_{,xx}; \tag{1}$$

$$\varepsilon_{\theta\theta} = \left(\frac{v_{,\theta}}{r} + \frac{wc}{r} + \frac{us}{r}\right) - z\left(\frac{w_{,\theta\theta}}{r^2} + \frac{w_{,x}s}{r} - \frac{v_{,\theta}c}{r^2}\right); \tag{2}$$

$$\gamma_{x\theta} = \left(\frac{u_{,\theta}}{r} + v_{,x} - \frac{vs}{r}\right) - z\left[\frac{w_{,\theta x}}{r} - \frac{w_{,\theta}s}{r^2} - \frac{c}{r}\left(\frac{v_{,x}}{2} - \frac{vs}{r}\right)\right]. \tag{3}$$

In accordance with the GBT, the mid-surface displacements *u*, *v*, and *w* are represented as a linear combination of orthogonal functions as follows:

$$u = \sum_{k=1}^{n} u_k(\theta) r(x) \phi_{k,x}(x); \quad v = \sum_{k=1}^{n} v_k(\theta) \phi_k(x); \quad w = \sum_{k=1}^{n} w_k(\theta) \phi_k(x). \tag{4}$$

In the above expressions, $u_k(\theta)$, $v_k(\theta)$, $w_k(\theta)$ are the cross-section displacement functions for mode *k*, while $\phi_k(x)$ is the corresponding modal amplitude function defined along the length.

2.2 Shell-type deformation modes

The conventional Generalized Beam Theory (GBT) typically assumes negligible shear strains $\gamma_{x\theta}^{M}$ and membrane transverse strains $\varepsilon_{\theta\theta}^{M}$. By utilizing Eqs. (1-4) the cross-section displacement components $v_k(\theta)$ and $w_k(\theta)$ can be determined based on the warping component

$u_k(\theta)$ (see Eq. (5)). Mention: the *us/r* and *–vs/r* components generally do not have a significant effect; therefore they are neglected in this formulation.

$$\gamma_{x\theta}^{M} = \left(\frac{u_{,\theta}}{r} + v_{,x}\right) = 0 \Rightarrow v_k = -u_{k,\theta}; \qquad \varepsilon_{\theta\theta}^{M} = \left(\frac{v_{,\theta}}{r} + \frac{wc}{r}\right) = 0 \Rightarrow w_k = -\frac{v_{k,\theta}}{c}. \tag{5}$$

To represent the displacement field for circular closed cross-sections, researchers have extensively used two independent sets of trigonometric functions which are given in Eq. (6), where *n* represents the number of shell-type modes that are considered [7]. Figure 2 presents the in-plane shapes of the first 12 shell-type deformation modes.

$$u_k = \begin{cases} \sin(m\theta), & m = \dfrac{k}{2}, \quad k = 2, 4, 6, \ldots, n; \\ \cos(m\theta), & m = \dfrac{k-1}{2}, \quad k = 3, 5, 7, \ldots, n+1. \end{cases} \tag{6}$$

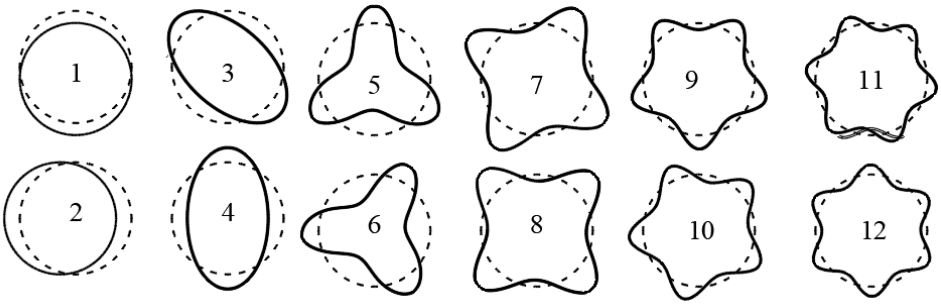

Figure 2. The shell-type deformation modes (in-plane shapes)

2.3 Shear deformation modes

Mureșan et al [8] recognized the limitations of Vlasov's hypothesis, namely the shear strains $\gamma_{x\theta}^{M} = 0$, and concluded that it leads to significant errors. Therefore, shear modes were also considered in this analysis as follows:

- "Shear u" modes: $v_k = w_k = 0$; u_k remains as described for shell-type modes (see Eq. (6));
- "Shear v-w" modes: $u_k = 0$; v_k and w_k remain as described for shell-type modes (see Eqs. (5)-(6)).

2.4 Additional deformation modes

Because of the assumptions adopted in section 2.2 (Eq. (5)), the shell and shear deformation modes are not able to describe three important types of deformation. Additional modes defined in previous research [7], [8] are introduced as follows :

- Axial extension mode: $u_e = 1$, $v_e = 0$, $w_e = 0$;
- Axisymmetric extension mode: $u_a = 0$, $v_a = 0$, $w_a = 1$;
- Torsion mode: $u_t = 0$, $v_t = r$, $w_t = 0$.

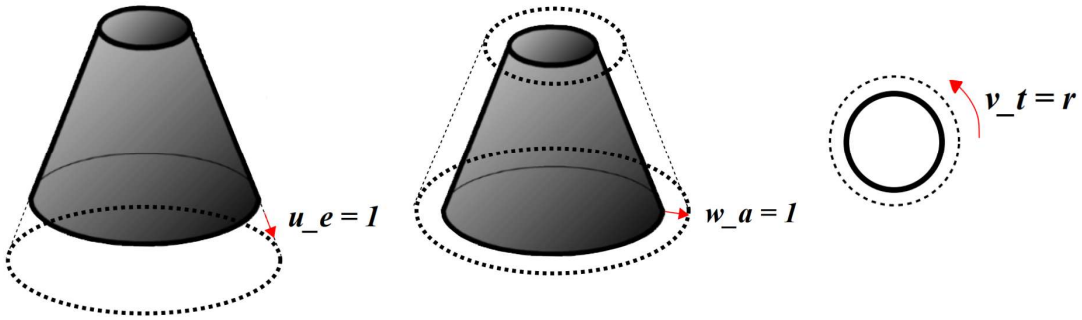

Figure 3: Additional deformation modes

2.5 FE formulation using GBT

The displacement field is obtained by using specific amplitude functions $\phi_k(x)$ associated with the known cross-section deformation modes. To approximate these amplitude functions, the polynomial shape functions proposed by Silvestre and Camotim [9] and Basaglia et al. [10] involving Lagrange and Hermite cubic polynomial primitives, are used in this paper. Using the kinematic relations given by Eqs. (1-3) and incorporating the shape functions, the relations between the strain components and the DOF vector ($\mathbf{q^e}$) at FE level, are found as follows:

$$\begin{Bmatrix} \varepsilon_{xx} \\ \varepsilon_{\theta\theta} \\ \gamma_{x\theta} \end{Bmatrix} = \begin{Bmatrix} B_{xx} \\ B_{\theta\theta} \\ B_{x\theta} \end{Bmatrix} q^e \tag{7}$$

where B_{xx}, $B_{\theta\theta}$, $B_{x\theta}$ are the "strain-DOF" matrices.

3 iFEM/GBT FORMULATION

iFEM finds the DOFs by minimizing the differences between theoretical strains $\mathbf{e}(\boldsymbol{q}) = \{\varepsilon_{xx}, \varepsilon_{\theta\theta}, \gamma_{x\theta}\}^T$ and the measured strains $\mathbf{e}^{\varepsilon}$. This is achieved through the minimization of a weighted least-squares functional Φ with respect to the nodal DOF.

$$\Phi(\boldsymbol{q}) = \|\mathbf{e}(\boldsymbol{q}) - \mathbf{e}^{\boldsymbol{\varepsilon}}\|^2 \tag{8}$$

The thin-walled element is discretized into longitudinal 1D inverse finite elements. For each finite element, a specific functional $\Phi_e(\mathbf{q^e})$ is defined as follows:

$$\Phi_e(q^e) = \frac{L_e}{n_\varepsilon} \sum_{i=1}^{n_\varepsilon} \left\{ \omega_{xx} \left[\varepsilon_{xx}(q^e)_{(i)} - \varepsilon^{\varepsilon}_{xx(i)} \right]^2 + \omega_{\theta\theta} \left[\varepsilon_{\theta\theta}(q^e)_{(i)} - \varepsilon^{\varepsilon}_{\theta\theta(i)} \right]^2 + \omega_{x\theta} \left[\gamma_{x\theta}(q^e)_{(i)} - \gamma^{\varepsilon}_{x\theta(i)} \right]^2 \right\} \tag{9}$$

where n_ε is the number of strain points within the FE and ω_{xx}, $\omega_{\theta\theta}$ and $\omega_{x\theta}$ are the weighting coefficients associated with the strain components (in this study, they are all equal to 1).

The least-squares functional is minimized with respect to DOF, giving rise to:

$$\boldsymbol{k^e q^e = f^e} \tag{10}$$

where $\boldsymbol{k^e}$ is the coefficient matrix and $\boldsymbol{f^e}$ is the constant terms vector depending on the measured strains.

$$\boldsymbol{k^e} = \sum_{i=1}^{n_\varepsilon} \left[B_{xx(i)} B_{xx(i)}{}^T + B_{\theta\theta(i)} B_{\theta\theta(i)}{}^T + B_{x\theta(i)} B_{x\theta(i)}{}^T \right] \tag{11}$$

$$\boldsymbol{f^e} = \sum_{i=1}^{n_\varepsilon} \left[\varepsilon^{\varepsilon}_{xx(i)} B_{xx(i)}{}^T + \varepsilon^{\varepsilon}_{\theta\theta(i)} B_{\theta\theta(i)}{}^T + \gamma^{\varepsilon}_{x\theta(i)} B_{x\theta(i)}{}^T \right] \tag{12}$$

The global system of equations $\boldsymbol{Kq} = \boldsymbol{F}$ is then assembled for the entire model, where $\boldsymbol{K}$ is a non-singular matrix that remains constant for a given distribution of FEs and strain points. The $\boldsymbol{F}$ vector is dependent on the measured strains and needs to be updated for each new measurement.

4 GBT MODAL IDENTIFICATION

This technique presented in [1] aims to identify the deformation modes that significantly influence the structure's behavior under the given loading and boundary conditions, and it relies on the orthogonality properties of the deformation modes, e.g., $\oint u_k u_i \, d\theta = 0$, for any $k \neq i$. A relatively large number of cross-section deformation modes is first proposed. Next, for each shell-type and additional mode, the integral of the product of the cross-section displacement functions is analytically computed as follows:

$$I_u = \oint u_k u_k \, d\theta, \; I_v = \oint v_k v_k \, d\theta, \; I_w = \oint w_k w_k \, d\theta \tag{13}$$

Next a shell FE model is constructed and after the analysis, the displacement field in the global coordinate system (U_{FE}, V_{FE}, W_{FE}) is extracted for all the nodes of the FE mesh. This global displacement field is then transformed into the local coordinate system, resulting in $u_{FE}(\theta, x)$, $v_{FE}(\theta,x)$, $w_{FE}(\theta,x)$. The modal amplitude functions $\phi_k(x)$ and their derivatives $\phi_{k,x}(x)$ in any cross-section j are found by numerical integration as follows:

$$\phi_k(x_j) = \frac{\oint v_k(\theta) v_{FE}(\theta, x_j) d\theta}{I_v} \text{ or}$$

$$\phi_k(x_j) = \frac{\oint w_k(\theta) w_{FE}(\theta, x_j) \, d\theta}{I_w} \tag{14}$$

$$\phi_{k,x}(x_j) = \frac{\oint u_k(\theta) u_{FE}(\theta, x_j) \, d\theta}{I_u}$$

5 IMPROVING THE SENSOR/FE CONFIGURATION FOR OPTIMAL RESULTS

The optimization of the sensor/FE configuration plays a important role in achieving reliable results in shape sensing. The process involves identifying the optimal number and locations of the sensor points. By following specific steps, the sensor/FE configuration can be refined to accurately represent the structural behavior efficiently. The procedure is next presented:

1. An analysis with shell-type finite elements is performed to extract strain and displacement fields (**e** and $\mathbf{U_{FE}}$) at FE nodes;
2. Modal identification is performed based on the displacement field to find the relevant GBT deformation modes;
3. An initial configuration of sensors and a 1D FE mesh are proposed;
4. The simulated measured strains e^{ε} are extracted in the sensor locations;
5. The relevant GBT deformation modes and simulated measured strains e^{ε} in the iFEM/GBT analysis are used to reconstruct the displacement field (U_{inv});
6. The reconstructed displacements (U_{inv}) are compared to the displacements from the shell FE analysis (U_{FE}) using the total displacements $U_t = \sqrt{U^2 + V^2 + W^2}$.
7. The error indicator is the maximum relative error. If the error indicator is less then a pre-specified tolerance, the final sensor configuration and 1D FE discretization are considered optimal. Otherwise, a new sensor/FE configuration is proposed and the analysis from step 4 is resumed.

6 DAMAGE DETECTION

The main objective of this paper is the detection of a potential damaged area of the analyzed conical member. The damage detection is performed by comparing the von Mises strains

distributions of the undamaged ($\varepsilon_{vm,undamaged}$) and damaged ($\varepsilon_{vm,damaged}$) members. The damage parameter D proposed by Li et al [5] is calculated as follows:

$$D = \left[\frac{\varepsilon_{vm,damaged} - \varepsilon_{vm,undamaged}}{\varepsilon_{vm,undamaged}}\right] \tag{15}$$

$$\varepsilon_{vm} = \frac{1}{\sqrt{2}}\sqrt{(\varepsilon_{xx} - \varepsilon_{\theta\theta})^2 + (\varepsilon_{xx} - \varepsilon_{zz})^2 + (\varepsilon_{\theta\theta} - \varepsilon_{zz})^2 + 6\gamma_{x\theta}{}^2} \tag{16}$$

$$\varepsilon_{zz} = \frac{\mu}{\mu - 1}(\varepsilon_{xx} + \varepsilon_{\theta\theta}) \tag{17}$$

where μ is Poisson's ratio.

7 NUMERICAL EXAMPLES

To validate the proposed formulation, three numerical examples are provided for thin-walled truncated cones, having the same geometry (length L=300 mm, minimum radius r_1=50mm, maximum radius r_2=100mm, thickness t=1 mm), and material properties (Young's modulus E=210 GPa and Poisson ratio μ = 0.3). All three members are fixed at the large radius end and free at the opposite end. Each example has different loading conditions.

The modeling of the members is done in Abaqus [11], employing shell S4R linear quadrilateral finite elements. There are 60 nodes on cross-section and 64 on the meridian, for all examples. After analysis, the simulated strains are extracted at the positions of the fictive strain sensors. The proposed iFEM/GBT formulation, modal identification and damage detection procedure are implemented using a Matlab [12] application. For the modal identification a tolerance value of 1% for the maximum relative error was chosen. The sensor/FE configuration was optimized using a tolerance value of 5%.

The damage is induced in the shell FE model in various positions, by reducing the Young's modulus in the damage region. This region covers a very small area given by four connected shell FEs. There are two damage cases, first a major reduction (E = 0.21 MPa) and then a minor reduction (E = 190 GPa). The proposed number of strain rosettes for which the deformed shape was successfully reconstructed is presented for each case together with the relevant deformation modes derived from the GBT modal identification. Differences between the total shell FE displacements and the reconstructed displacements are highlighted. Subsequently, the damage parameter D is presented on the entire surface in two approaches: (i) using the strains extracted from Abaqus and (ii) using the strains reconstructed using the iFEM/GBT methods.

7.1 Member under uniformly distributed axial load

Resultant of the distributed load, P=32.5 kN;
Number of sensors = 40.

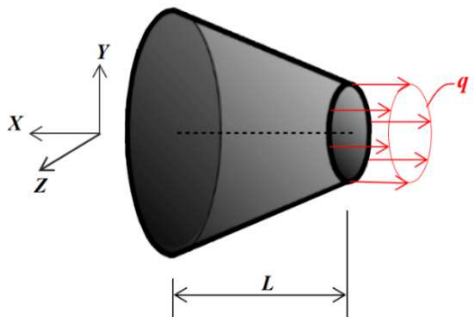

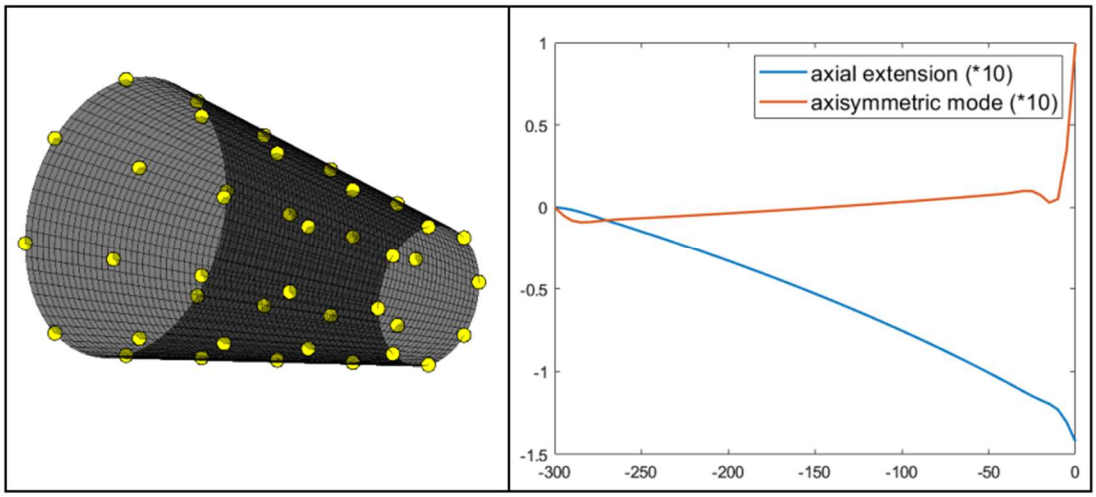

Figure 4: Sensor configuration and significant deformation modes

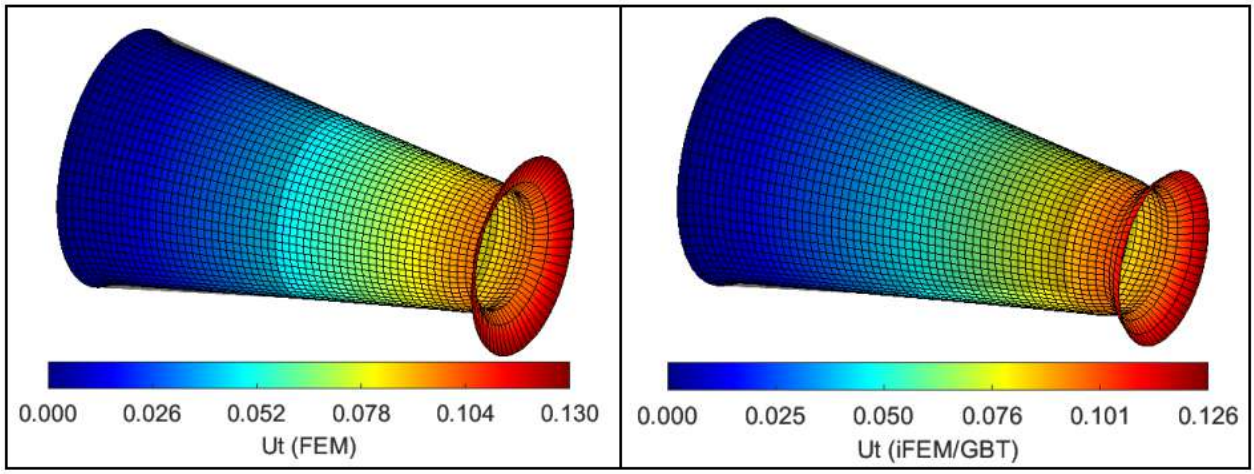

Figure 5: Contour plots of U_t displacements (FEM vs. iFEM/GBT)

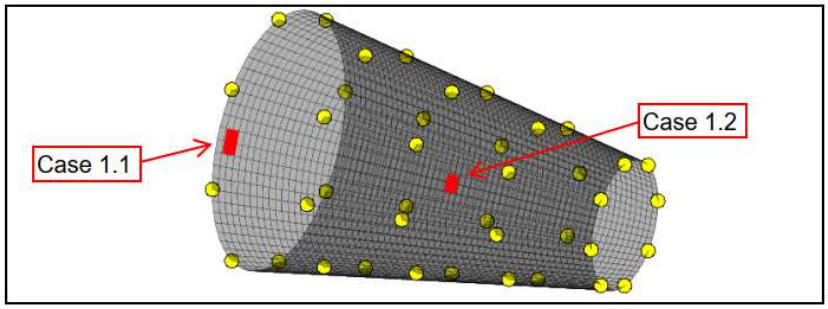

Figure 6: Proposed damaged location for Case 1.1 and 1.2

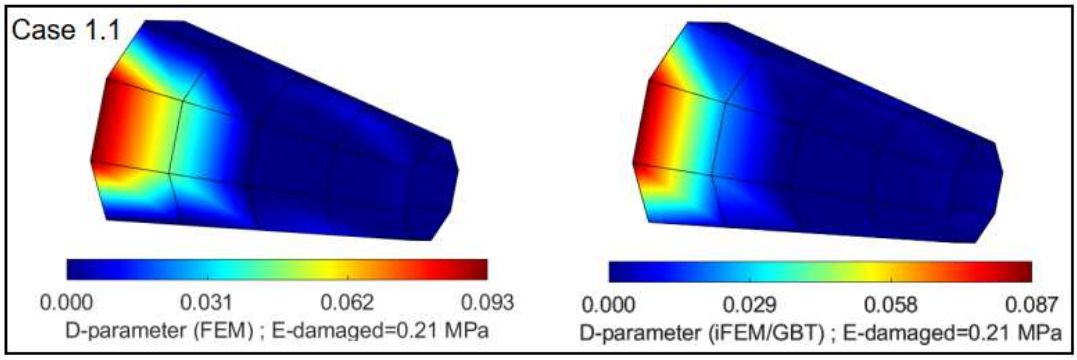

Figure 7: Damage detection (FEM vs. iFEM/GBT) – Case 1.1

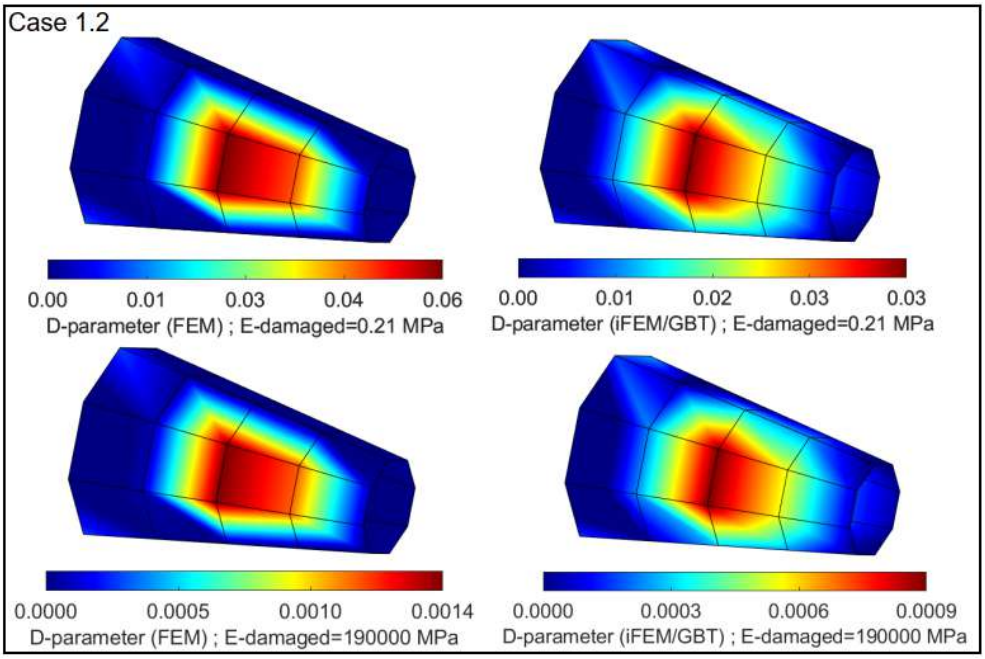

Figure 8: Damage detection (FEM vs. iFEM/GBT) – Case 1.2

7.2 Member under end loads

F - loads: F_x=-5kN; F_y=5kN; F_z=15kN;
M - loads: M_x=-1kNm; M_y=2kNm; M_z=2kNm;
Number of sensors = 56.

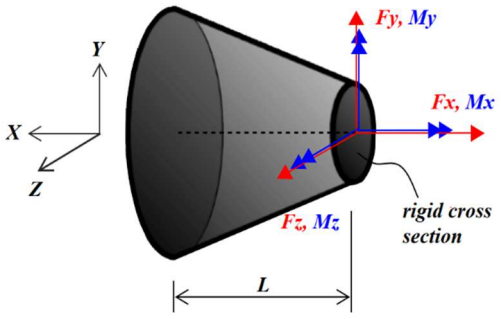

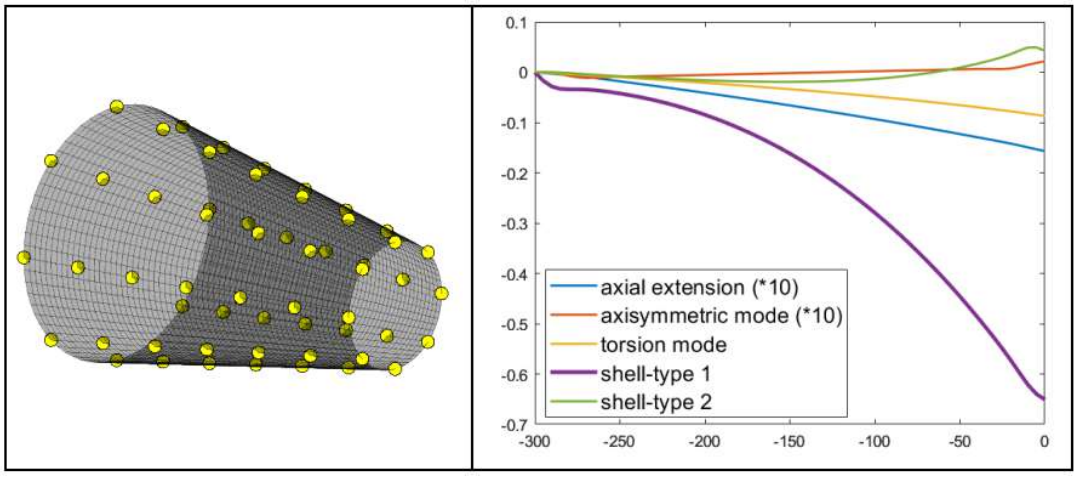

Figure 9: Sensor configuration and significant deformation modes

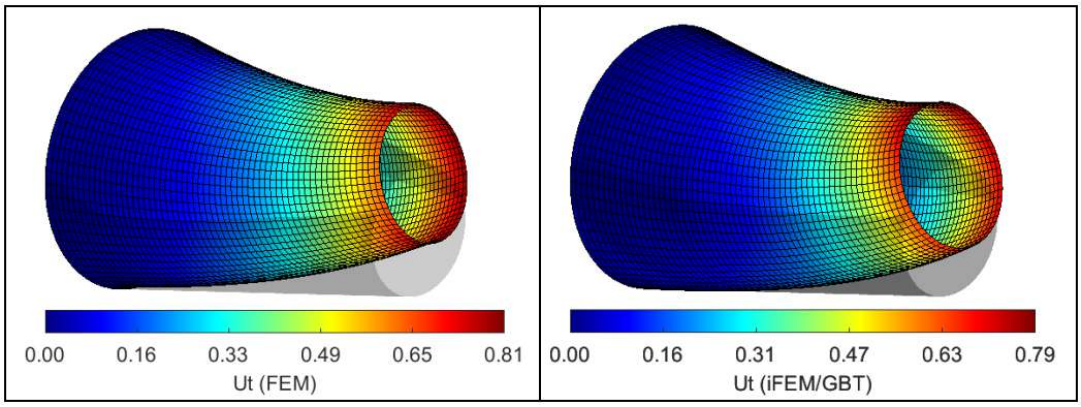

Figure 10: Contour plots of U_t displacements (FEM vs. iFEM/GBT)

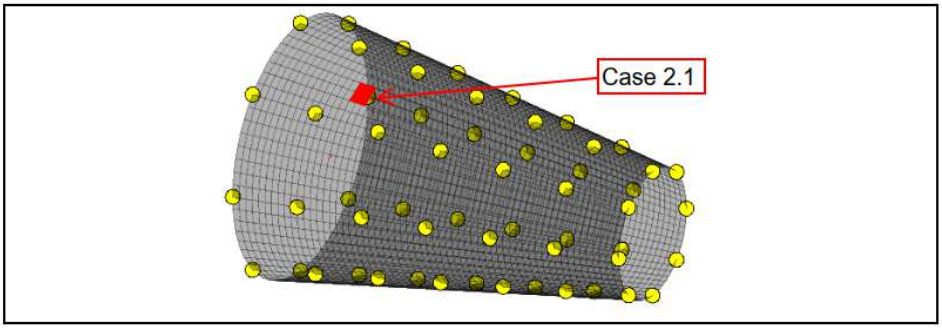

Figure 11: Proposed damaged location for Case 2.1

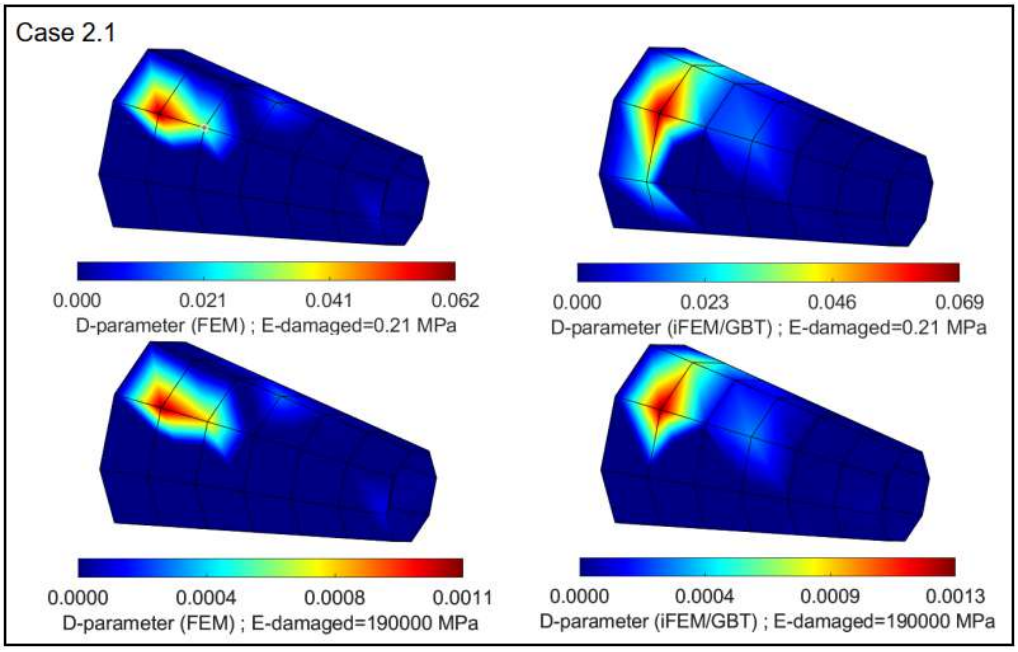

Figure 12: Damage detection (FEM vs. iFEM/GBT) – Case 2.1

7.3 Member under uniformly distributed transverse load

Load: q = 2 kN/m;

Because of the symmetry plane of this structure (Oxy), it is possible to conduct iFEM/GBT analysis on only one half of the truncated cone. Thus, 35 sensors (for shape sensing) and 77 sensors (for damage detection) were placed on the half of the geometry.

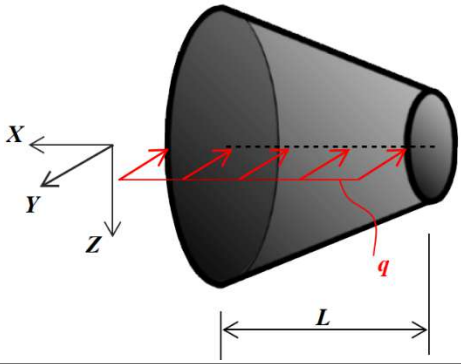

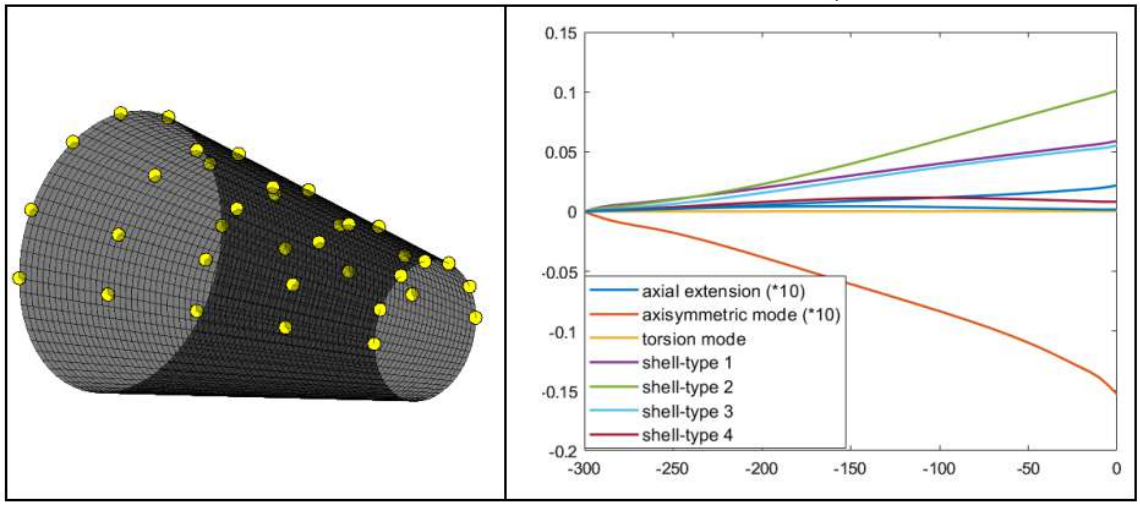

Figure 13: Sensor configuration (for shape sensing) and significant deformation modes

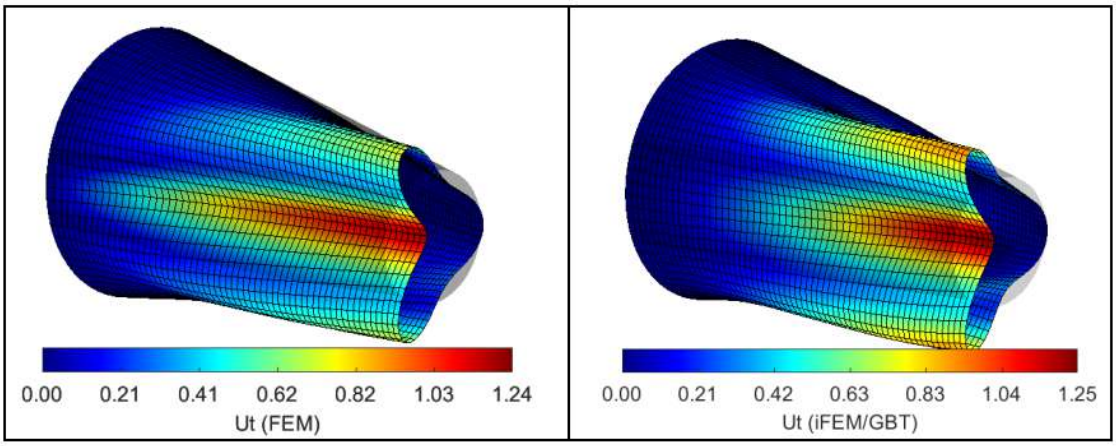

Figure 14: Contour plots of U_t displacements (FEM vs. iFEM/GBT)

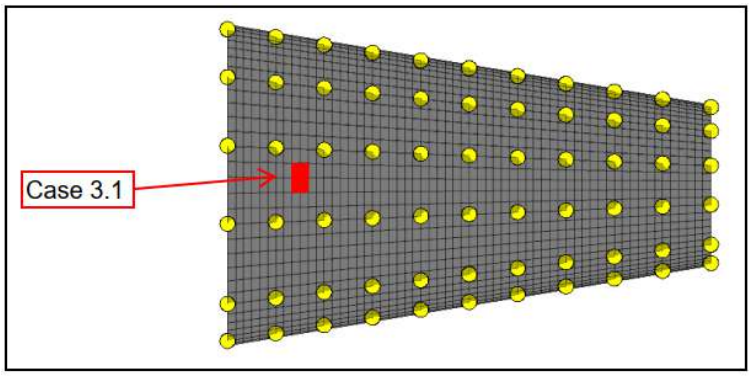

Figure 15: Sensor configuration (for damage detection) and damage location for Case 3.1

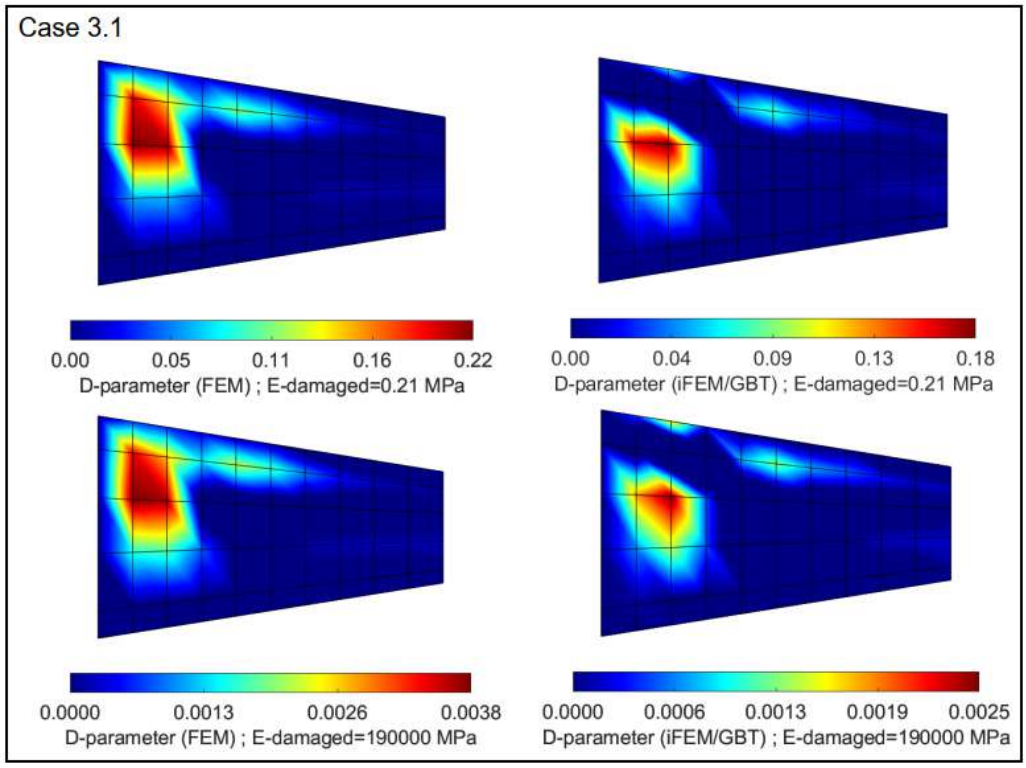

Figure 16: Damage detection (FEM vs. iFEM/GBT) – Case 3.1

8 CONCLUSIONS

Analyzing the illustrations from the numerical examples, it can be seen that the method proposed by combining iFEM and GBT offers satisfactory results regarding the shape sensing and the detection of the potential damage.

For case 7.1 and case 7.2 both shape sensing and damage detection led to good results with the same number of sensors (40 and 56, respectively). For case 7.3 (member under uniformly distributed transverse load) the shape sensing required 35 strain sensors, but to detect the damage, an increase in the number of sensors, along the length, was imposed due to the variation of the strains for this type of loading. A gratifying aspect is the fact that for all cases, a very small damage surface was detected (approximately 2 cm^2), both for the drastic reduction of the Young's modulus (E = 0.21 MPa) and for a reduction of only 10% (E = 190 000 MPa).

The accuracy of the method was validated by comparison with the results obtained from the shell FEM analysis regarding displacements and damage parameters.

REFERENCES

[1] Nedelcu M., Optimisation of inverse Finite Element Method for shape sensing of thin-walled cylinders by using Generalised Beam Theory, *Thin-Walled Structures*, 188, 110865, 2023.

[2] Tessler A., Spangler J.L., A variational principle for reconstruction of elastic deformation of shear deformable plates and shells, *NASA TM-2003-212445*, 2003.

[3] Tessler A., Spangler J.L., A least-squares variational method for full-field reconstruction of elastic deformations in shear-deformable plates and shells, *Comput. Methods Appl. Mech. Eng.* 194 (2), 327–339, 2005.

[4] Schardt R., Verallgemeinerte Technische Biegetheorie, *Springer Verlag*, Berlin, 1989 (in German).

[5] Li M., Kefal A., Cerik B.C., Oterkus E., Dent damage identification in stiffened cylindrical structures using inverse Finite Element Method, *Ocean Eng* 198, 106944, 2020.

[6] Goldfeld Y., Imperfection sensitivity of laminated conical shells, *Solids and Structures*, 44 (2007) 1221–1241.

[7] Silvestre N., Generalised beam theory to analyse the buckling behaviour of circular cylindrical shells and tubes, *Thin-Walled Structures*, 45 (2), 185–198, 2007.

[8] Mureşan A., Nedelcu M., Gonçalves R., GBT-based FE formulation to analyse the buckling behaviour of isotropic conical shells with circular cross-section, *Thin-Walled Structures*, 134, pp. 84-101, 2019.

[9] Silvestre N., Camotim D., Non-linear generalized beam theory for cold-formed steel members. *Struct. Stab. Dyn*. 3 (4), 461–490, 2003.

[10] Basaglia C., Camotim D., Silvestre N., Non-linear GBT formulation for open-section thin-walled members with arbitrary support conditions. *Comput. Struct*. 89 (21–22), 1906–19, 2011.

[11] ABAQUS Standard (Version 6.3), 2002, Hibbit Karlsson and Sorensen Inc.

[12] Matlab 2005. Version 7.1.0246 Documentation, The Mathwork Inc